Journal of Alloys and Compounds 480 (2009) 428–433

Contents lists available at ScienceDirect

Journal of Alloys and Compounds

journal homepage: www.elsevier.com/locate/jallcom

Pressure–composition–temperature hysteresis in C14 Laves phase alloys: Part 1. Simple ternary alloys

K. Young*, T. Ouchi, M.A. Fetcenko

Energy Conversion Devices Inc., 2983 Waterview Drive, Rochester Hills, MI 48309, USA

ARTICLE INFO

Article history:
Received 14 November 2008
Received in revised form 16 December 2008
Accepted 23 December 2008
Available online 4 January 2009

Keywords:
Hydrogen absorbing materials
Transition metal alloys and compounds
Metal hydride
Thermodynamic properties

ABSTRACT

In Part 1 of a series of two papers, the a/c lattice constant ratio of $ZrCr_2$-based ternary alloys are shown to be strongly correlated not only to the number of outside electrons of substitutional elements but also to the PCT absorption/desorption hysteresis and the degree of pulverization during hydride/dehydride cycling of the alloy. In differentiation from AB5 alloys in which elongating the c-axis dimension of the unit cell extends the alloy's electrochemical cycle life, flattening the unit cell of an AB2 alloy extends its cycle life. This difference can be explained by the different hydrogen occlusion sites of the two structures. Adding small amounts (10%) of substituents such as Zn, Cr, Mo, Si, or Cu, was generally found to help the prevention of the alloy hydride/dehydride pulverization by maintaining a relatively high a/c lattice constant ratio. Application of these principles to more complicated electrochemical hydrogen storage alloys can be found in Part 2 of this series.

1. Introduction

Ever since Ubbelohde suggested the extra degree of freedom from internal strain as the origin of hysteresis in pressure–concentration–temperature (PCT) isotherms of hydrogen storage metals such as Pd [1], there has been a long history of studies on the causes of PCT hysteresis. Through the years, two models have been applied successfully in fitting the experimental data under different conditions. At relatively low temperatures (compared to the melting point), a plastic deformation model was constructed based on the irreversible energy losses in the vicinity of growing hydride particulates in the metal matrix [2–4]. Alternatively, at higher temperatures, where the deformed structure should be recovered within a short period, a coherent elastic model was presented to introduce an energetic barrier between the metastable hydrogen solid solution (α-phase) and the stable hydride (β-phase) [5–8]. Other previously presented models have been based upon (a) dislocations formed during both the hydride and dehydride processes [9,10]; (b) a metastable phase from oversaturating the α-phase [11]; (c) a miscibility gap [12]; (d) mathematical models [13,14]; and (e) hydrogen–metal and hydrogen–hydrogen interaction kinetics [15]. Comprehensive reviews on various types of theoretical models were presented by Northwood [16], Flanagan [17] and their coworkers.

There are generally two families of hydrogen storage alloys used in nickel metal hydride (NiMH) Batteries, namely rare earth based AB5 and Laves phase based AB2. Close relationships between PCT hysteresis and degree of pulverization of the $LaNi_5$-based AB5 alloys—$LaNi_{5-x}Al_x$ and $MmNi_{5-x}B_x$ (B = Al, Zr, Mn, Cr, and Co) have been previously reported [18]. A smaller PCT hysteresis corresponds to a lower degree of pulverization during gas phase hydride/dehydride cycling. An explanation for this correlation is that the building of internal stress from the PCT hysteresis causes particles to fracture during hydriding. The connection between PCT hysteresis and some structural parameters, such as lattice constants, was established for the AB5 alloy family by Osumi et al. [19]. A higher c/a lattice constant ratio leads to a smaller lattice expansion during hydriding and less stress, causing a smaller PCT hysteresis and a low degree of pulverization during gas phase hydride/dehydride cycling.

The main working phases for AB2 alloys in NiMH battery applications are the C14 (hexagonal) and the C15 (face-centered-cubic) Laves phases [20–22]. Since no distortion of the cubic unit cell of the C15 structure occurs, no correlation exists between the lattice parameters of the C15 structure and its PCT hysteresis. For example, for the alloy $Zr_{1-x}Ti_xNi_{1.3}Mn_{0.7}$ (C15 structure), the PCT hysteresis increases as the lattice constant a increases, while in another C15 alloy, $ZrNi_{1.3}Mn_{0.7-y}V_y$, the PCT hysteresis decreases as the lattice constant a increases [23]. Unlike the C15 structure, the C14 structure has a deformable unit cell (i.e. the a/c ratio can vary) similar to the $CaCu_5$ structure in AB5 alloys. It should be noted that the hydrogen occupation site positions are very different for the C14 and $LaNi_5$ structures (Fig. 1). Therefore, a close examination of the relation-

* Corresponding author. Tel.: +1 248 293 7000; fax: +1 248 299 4520.
E-mail address: kwoyoung@yahoo.com (K. Young).

0925-8388/$ – see front matter © 2009 Elsevier B.V. All rights reserved.
doi:10.1016/j.jallcom.2008.12.113

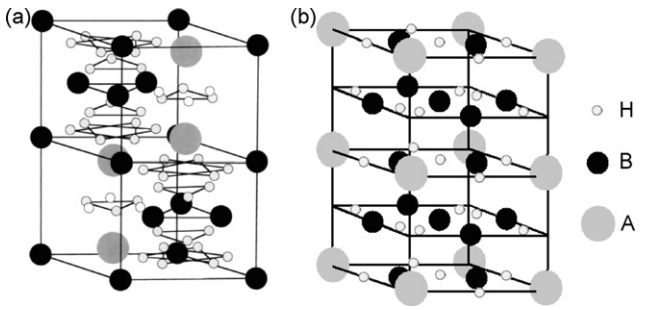

Fig. 1. Schematic drawings of the hydride crystal structures of AB2 C14 (a) and AB5 $LaNi_5$ (b). Small circles represent possible interstitial sites for hydrogen storage. These models are after Refs. [24,25].

ship between PCT and hysteresis in the C14-Laves based AB2 alloy would be of scientific interest.

Ni is the major B element used in both AB2 and AB5 electrode alloys. However, neither $ZrNi_2$ nor $TiNi_2$ are available in the stable intermetallic form. Therefore, in the first part of this two-part paper, we chose a simple binary alloy, $ZrCr_2$, as the base alloy for studies of the elemental substitution effects on lattice constants, the pulverization rate, the PCT hysteresis, and correlations between these parameters. The $ZrCr_2$ base alloy was chosen for: (a) its simple C14 crystal structure [24]; (b) its high hydrogen storage capacity [25–27]; (c) its large PCT hysteresis; and (d) the extensive studies on structural, thermodynamic, and electronic properties [28–31], and many studies on elemental substitution that have been performed (i.e. Ti [32,33], V [34–39], Mn [37,40], Fe [37,40–48], Co [37,40,41,47,49], Ni [37,40,47,50–54], Cu [37,40,55], Mo [37,38], Mo [38,56], Al [57], Si, and Ge [58]).

2. Experimental setup

Research grade raw materials (purity > 99.9%) were weighed according to the target compositions listed in Table 1. Arc melting was performed under flowing argon with a non-consumable tungsten electrode and a water-cooled copper tray. Before each arc melt, a piece of sacrificial titanium underwent a melting–cooling cycle a few times to reduce the residual oxygen concentration. Each 5-g ingot was re-melted and turned over a few times to ensure uniformity in the chemical composition. The chemical composition of each sample was examined by a Varian *Liberty* 100 inductively coupled plasma (ICP) system. A Philips *X'Pert Pro* X-ray diffractometer (XRD) was used to study the microstructure. PCT analysis and gas phase cycling were performed with a Suzuki–Shokan multi-channel PCT system. In the PCT analysis, each sample was first activated by a 2-h thermal cycle between 300 °C and room temperature at 25 atm H_2 pressure. The hydride/dehydride cycling was performed in the following conditions: (1) ramping up the hydrogen pressure to 2 MPa in 3 min; (2) maintaining that pressure for 1 min; (3) ramping down the hydrogen pressure to 0.2 MPa in 2 min; and (4) venting with a vacuum pump for 1 min. A Horiba La-300 Laser Scattering Particle Size Analyzer was used to measure the particle size distribution.

3. Results and discussion

Twelve alloys with chemical compositions listed in Table 1 were made by arc melting. Sample ZC-1 was the $ZrCr_2$ base binary alloy while the others were ternary alloys with 10% of the chromium replaced by substituents, such as Mo (ZC-2), Mn (ZC-3), Ni (ZC-4), Al (ZC-5), Co (ZC-6), V (ZC-7), Cu (ZC-8), Si (ZC-9), Zn (ZC-10), Sn (ZC-11), and Fe (ZC-12). The average composition of the resulting ingot was verified by ICP to be within 0.1 wt.% from the target. XRD analysis was performed on the powder after grinding each alloy ingot and the resulting spectra are plotted in Fig. 2. Except for sample ZC-7 which has a predominantly C15 structure, the alloy samples have predominantly C14 crystal structures. No phases other than the Laves C14, C15, and C36 structures were observed. These XRD results are consistent with the previous reports on $ZrCr_2$ partially substituted by V, Mn, Fe, Co, Ni, Cu, and Mo [37].

Table 1
Summary of compositions, atomic radius of substituting element, lattice parameters, PCT gas phase characteristics for alloys in this study.

	Composition	Atomic radius[a] (Å)	a (Å)	c (Å)	a/c	Unit cell vol. (Å^3)	Max. Cap. (wt.%)	2/3P-abs (atm)	2/3P-des (atm)	Hys@ 2/3 storage	Ave. size after 100 cycles (μm)	Percentage of size less than 30 μm
ZC-1	$ZrCr_2$	1.423	5.1224	8.3061	0.6167	188.74	1.49	0.22	0.20	0.11	91.2	10.0
ZC-2	$ZrCr_{1.8}Mo_{0.2}$	1.550	5.1540	8.3394	0.6180	191.84	1.71	0.14	0.12	0.15	71.7	17.2
ZC-3	$ZrCr_{1.8}Mn_{0.2}$	1.428	5.1074	8.3261	0.6134	188.09	1.73	0.06	0.05	0.24	48.2	32.9
ZC-4	$ZrCr_{1.8}Ni_{0.2}$	1.377	5.0923	8.3296	0.6113	187.06	1.53	0.08	0.07	0.15	47.3	26.8
ZC-5	$ZrCr_{1.8}Al_{0.2}$	1.582	5.1362	8.3801	0.6129	191.45	1.31	0.10	0.08	0.18	40.2	40.2
ZC-6	$ZrCr_{1.8}Co_{0.2}$	1.385	5.0875	8.3320	0.6106	186.76	1.15	0.17	0.10	0.52	45.6	27.9
ZC-7	$ZrCr_{1.8}V_{0.2}$	1.491	5.1258	8.3404	0.6146	189.77	1.31	0.09	0.09	0.07	34.1	52.3
ZC-8	$ZrCr_{1.8}Cu_{0.2}$	1.413	5.1117	8.3133	0.6149	188.11	1.40	0.08	0.07	0.09	83.0	11.9
ZC-9	$ZrCr_{1.8}Si_{0.2}$	1.669	5.1151	8.3227	0.6146	188.58	0.95	0.35	0.29	0.18	160.0	4.0
ZC-10	$ZrCr_{1.8}Zn_{0.2}$	1.538	5.1261	8.3042	0.6173	188.97	1.25	0.13	0.11	0.16	249.6	1.8
ZC-11	$ZrCr_{1.8}Sn_{0.2}$	1.862	5.1633	8.4381	0.6119	194.81	1.32	0.06	0.04	0.31	27.1	68.2
ZC-12	$ZrCr_{1.8}Fe_{0.2}$	1.411	5.0945	8.3358	0.6112	187.36	1.56	0.08	0.06	0.28	48.2	26.4

[a] The atomic radius here is from the substitutional atom [59]. In the case of ZC-1, atomic radius is from Cr.

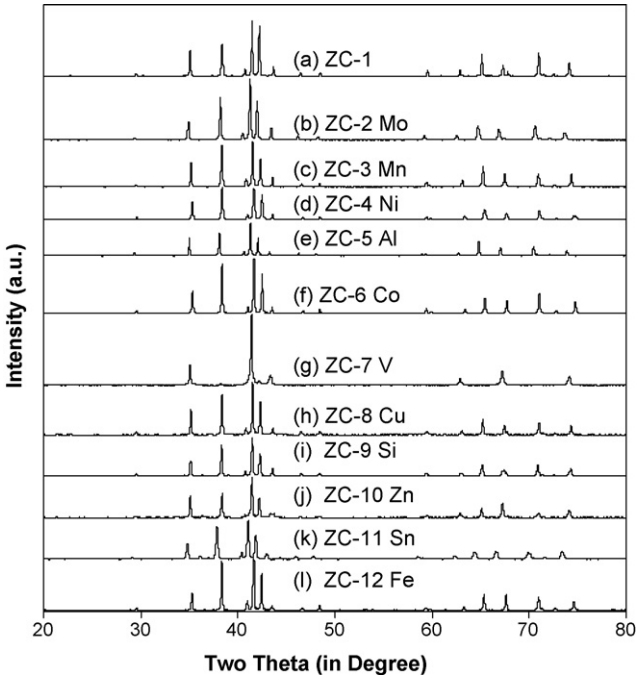

Fig. 2. XRD spectra using Cu K_α as the radiation source for alloys ZC-1 to ZC-12. Only ZC-7 alloy shows a predominantly C15 structure while others show predominantly C14 structures.

Both the average electron concentration (AEC) [60,61] and the ratio of average electron radii (RAER) between A-site elements and B-site elements have been previously used to predict the preferential structure (i.e. C14, C15) [62]. For the alloys of the present study, AEC predicts that a substituent with fewer outer shell electrons, such as V, will have a tendency to form a C15 structure, which has been observed in our case. However, the RAER predicts that a substituent with a larger atomic radius will preferentially form a C15 structure, which has not been seen here. Therefore, the AEC value is more reliable in predicting the preference of Laves phases than the RAER value is in the case of $ZrCr_2$-based alloys.

Both lattice constants a and c of the C14 lattice structure, together with their ratio for each alloy, were calculated from the alloy's XRD spectrum and are listed in Table 1. Depending on the substituent, both a and c values can be increased or decreased. In the case of ZC-7 (partially V-substituted), both lattice constants a and c are increased, which confirms that the V atoms occupy B-sites, as was previously reported [38]. Moving across the periodic table from left to right, the corresponding substituent elements V, Cr, Mn, Fe, Co, Ni, Cu, and Zn cause the a/c ratio to first decrease (from the base alloy) and then to increase. This trend is shown in Fig. 3 and is similar to the evolution of atomic radius with the atomic number and indicates the possible linkage between a/c ratio and the number of outer shell electrons. The unit cell volumes, calculated from the a and c lattice constants, are also listed in Table 1 and plotted against the atomic radius of the substituent in Fig. 4. In general, a larger substituent increases the unit cell volume. A linear correlation can be set up with the exception of ZC-9 with Si-substitution, which is a non-transition metal element.

Lattice constants a and c for $ZrCr_2$ partially substituted with different amounts of Mo and Ni have been previously reported [53,56]. For $ZrCr_{2-x}Mo_x$, increases in x from 0 to 0.2, 0.4, 0.8 to 1.0, correspond to a/c ratios 0.6156, 0.6161, 0.6159, 0.6157, and 0.6172. The initial trend for x from 0 to 0.2 is the same as our present result. When more Mo was added, a/c values declined by a small amount and then jumped to a maximum when $x = 1.0$. In the case of Ni substitution, when x in $ZrCr_{2-x}Ni_x$ increases from 0 to 0.2, 0.4, 0.6 to 0.8, the corresponding a/c ratios are 0.6156, 0.6123, 0.6101, 0.6099, and 0.6106. Again, the initial trend from $x = 0$ to 0.2 is the same as ours. As more Ni was added, the a/c value continued to decline until x reached 0.8, where a small increase in a/c value was observed. In all cases, Mo was found to increase a/c ratios and Ni was found to decrease a/c ratios at any level of substitution.

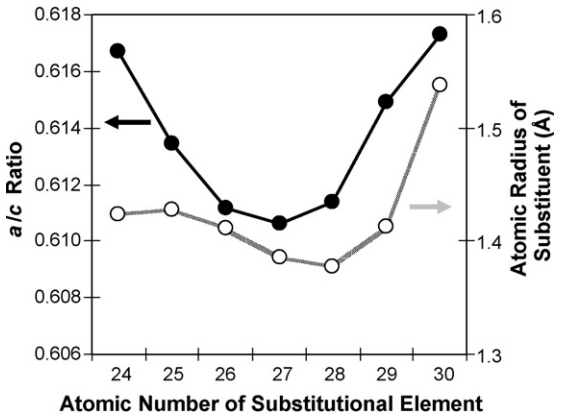

Fig. 3. Plot of ratios of a and c lattice constants measured by XRD and atomic radii vs. atomic numbers of substituents.

PCT isotherms of ZC-1 at three different temperatures (90 °C, 120 °C, and 150 °C) were measured and are plotted in Fig. 5. A large absorption/desorption hysteresis was observed in the 90 °C isotherm. The hysteresis reduced substantially at higher temperatures, which seems to agree with the energy barrier hypothesis [5–8]. In absorption isotherms, three plateaus corresponding to hydrides with different metal–hydrogen bond strengths were observed. At the lowest pressure region in our study (~0.001 MPa), only the hydride with the weakest M–H bond strength could be fully dehydrided at a temperature below 150 °C. Therefore, in the following calculation of PCT hysteresis, we only focus on the hydride phase with the highest plateau pressure and define the hysteresis at two thirds of the full storage capacity, which is about the middle of the highest plateau. Heat of hydride formation and change in entropy were calculated from pressures at 1% storage capacity for the 120 °C and 150 °C isotherms. The corresponding results are −30.1 kJ/mol H_2 and −82.5 kJ/mol H_2. Because of the lack of a well-defined plateau in these PCT isotherms, this heat of formation deviates from both the measured value (−46.0 kJ/mol H_2 in [63]) and the calculated value (−40.1 kJ/mol H_2 following Eq. (10) of [13]).

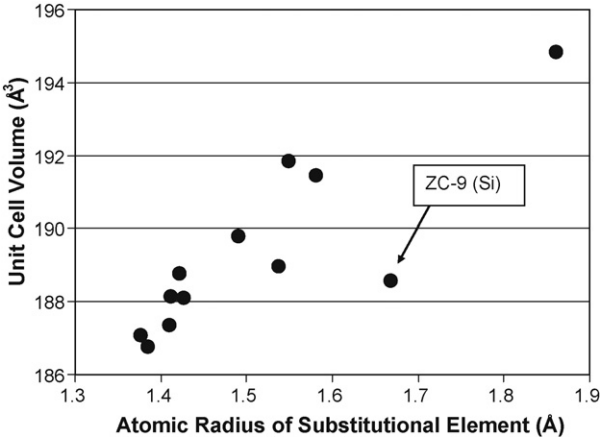

Fig. 4. Plot of unit cell volume calculated from XRD lattice constants vs. atomic radii of substituents.

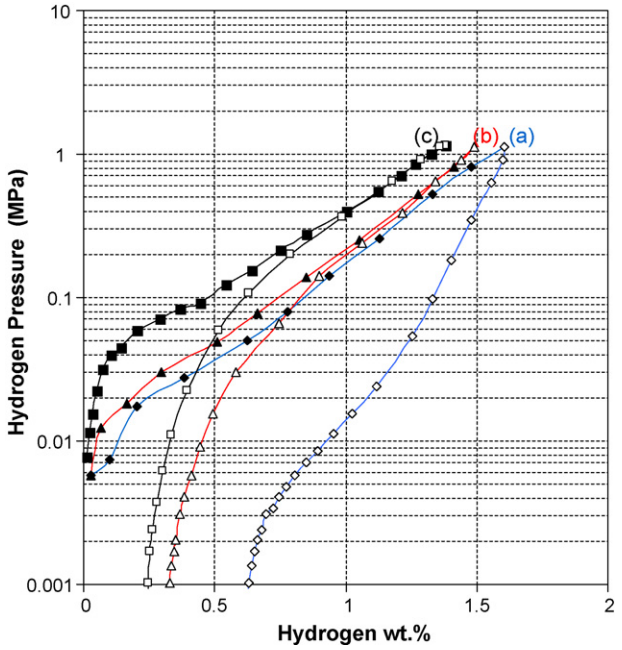

Fig. 5. PCT absorption and desorption isotherms measured at (a) 90 °C, (b) 120 °C, and (c) 150 °C for alloy ZC-1 (base $ZiCr_2$). Absorption and desorption points are represented by solid and open symbols respectively.

PCT isotherms for alloys ZC-2 to ZC-12 measured at 120 °C are plotted in Figs. 6–8. Table 1 lists the full capacity, absorption and desorption pressures at two-thirds of full capacity, as well as the hysteresis, which is defined as

$$\text{Hys} = \ln \frac{P_{a \text{ at } 2/3 \text{ capacity}}}{P_{d \text{ at } 2/3 \text{ capacity}}}.$$

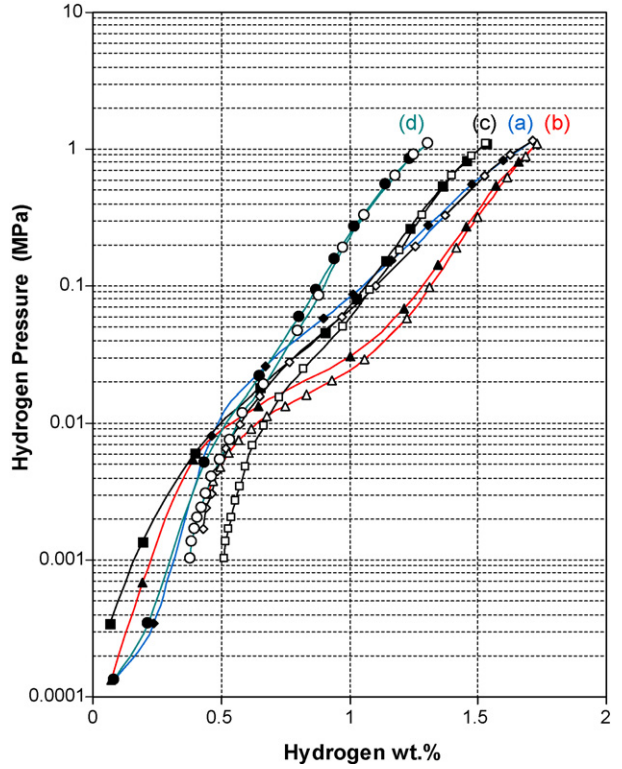

Fig. 6. PCT absorption and desorption isotherms measured at 120 °C for alloys ZC-2 (a), ZC-3 (b), ZC-4 (c), and ZC-5 (d). Absorption and desorption points are represented by solid and open symbols respectively.

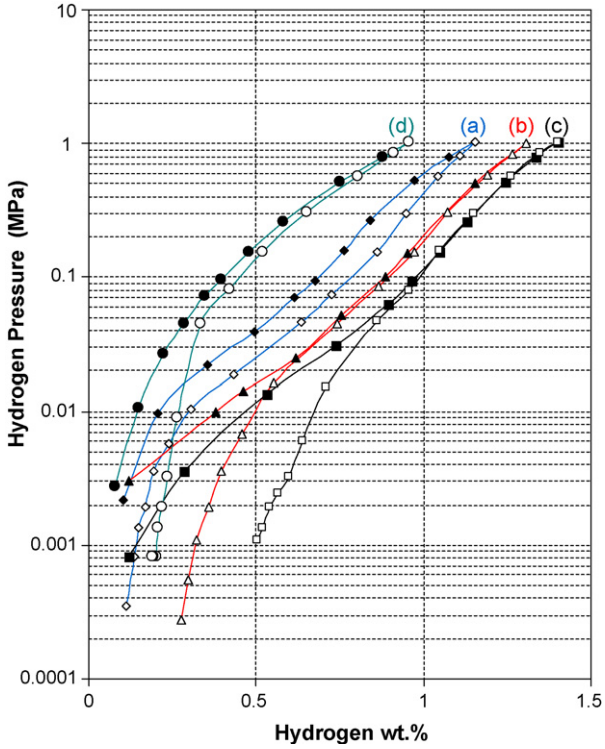

Fig. 7. PCT absorption and desorption isotherms measured at 120 °C for alloys ZC-6 (a), ZC-7 (b), ZC-8 (c), and ZC-9 (d). Absorption and desorption points are represented by solid and open symbols respectively.

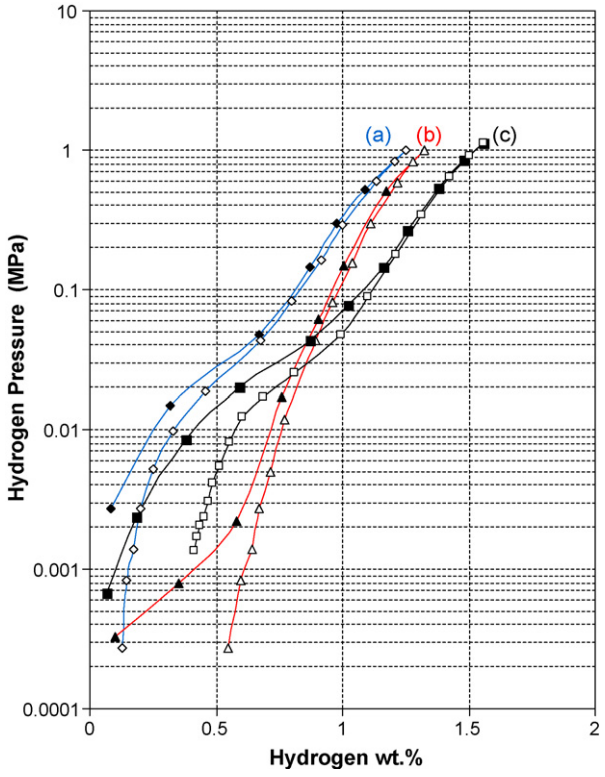

Fig. 8. PCT absorption and desorption isotherms measured at 120 °C for alloys ZC-10 (a), ZC-11 (b), ZC-12 (c). Absorption and desorption points are represented by solid and open symbols respectively.

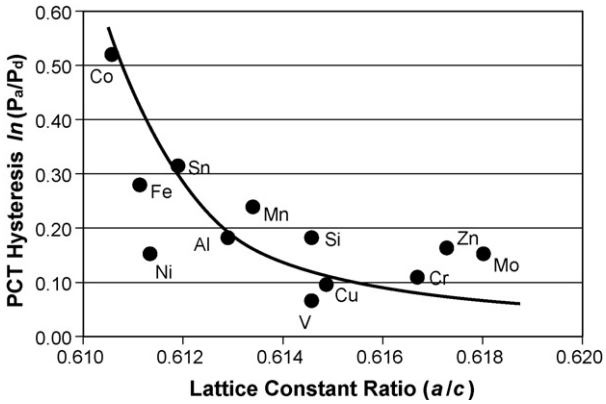

Fig. 9. Plot of the PCT hysteresis measured at 2/3 of full storage capacity vs. lattice constant ratios a/c. A trendline indicates a higher a/c ratio reducing the PCT hysteresis.

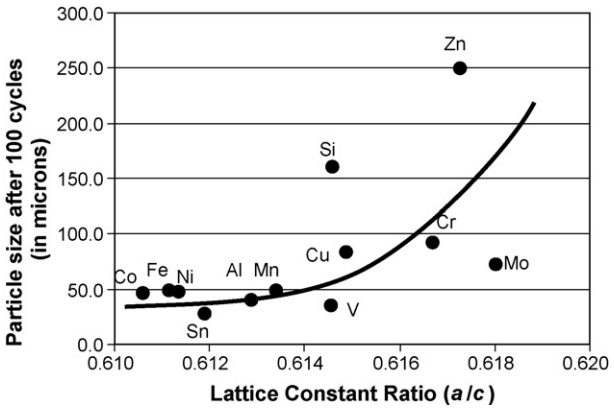

Fig. 11. Plot of the average particle size (mean by volume) after 100 hydride/dehydride cycles vs. lattice constant ratio a/c. A trendline indicates a higher a/c ratio corresponding to a lesser degree of pulverization.

These Hys values are plotted against the corresponding lattice constant a/c ratios in Fig. 9. The trendline indicates that a larger a/c ratio corresponds to a small Hys value. This correlation is opposite to that of AB5 alloy systems [19]. In the AB5 hydride structure, the possible hydrogen occlusion sites are aligned on the same plane that the A and B atoms reside (Fig. 1b). A taller unit cell (larger c/a ratio) will bring hydrogen sites closer together and make the proton hopping easier, thereby lowering the energy barrier across the α–β-phase boundary during hydriding and reducing the PCT hysteresis. In the C14 hydride structure, none of the hydrogen occlusion sites are aligned in the same plane with either A or B atoms, which makes the shortest hopping path along the c-axis. Therefore, a flatter unit cell (larger a/c ratio) in C14 structure will decrease the distance between hopping sites and reduce the PCT hysteresis.

In order to establish the correlation of PCT hysteresis and degree of pulverization, all alloys went through 100 hydride/dehydride cycles, and the particle distributions of the resulting powder were analyzed. Four representative particle distributions from alloys ZC-1, ZC-9, ZC-10, and ZC-12 are plotted in Fig. 10. Both the average particle size (mean by volume) and percentage of powder less than 30 μm for each alloy are listed in Table 1. A smaller average particle size in general corresponds to a higher percentage of fine particles. Average particle size of C14-predominated alloys is plotted against a/c ratio in Fig. 11. A higher a/c ratio corresponds to a larger average particle size, which means a lower degree of pulverization. In Fig. 12, the percentage of powder particles less than 30 μm in size is plotted against the a/c ratio for all C14-predominated alloys. This plot confirms that a larger a/c ratio corresponds to fewer fine particles. This finding is consistent with studies performed for the AB5 alloy: a high PCT hysteresis indicates an increased amount of barrier energy between α and β-phases of the hydride and causes a higher degree of pulverization during hydride/dehydride cycling. In the case of C15-predominated ZC-7, although its PCT hysteresis is smaller than any alloy from the C14-predominated group, its pulverization rate is worse than that from any other C14 alloys except for the Sn-substituted ZC-11.

Lattice constants a (5.4191 Å) and c (8.8670 Å) were calculated from the XRD spectrum of a fully hydrided ZC-1 sample (base $ZrCr_2$). The lattice expansion of the hydride along the c-axis (6.8%) is higher than that along the a-axis (5.8%). This trend is consistent with the 6.5% and 5.5% lattice expansions along the c- and a-axes of $ZrCr_2$ as previously reported [40,56]. The preferred expansion orientation is just the opposite for $LaNi_5$ structure as can be seen from the larger expansion in a parameter than c parameter when x in $LaNi_5H_x$ is less than 6 [64]. This difference can be explained by our earlier argument that positions of hydrogen occlusion sites are different for the C14 and $LaNi_5$ cell structures. While the hydrogen in $LaNi_5$ system resides in the a–b plane and causes a larger expansion in the "in-plane" lattice constant a, the hydrogen in C14 occupies sites along the c-axis and results in a larger expansion in the c lattice constant.

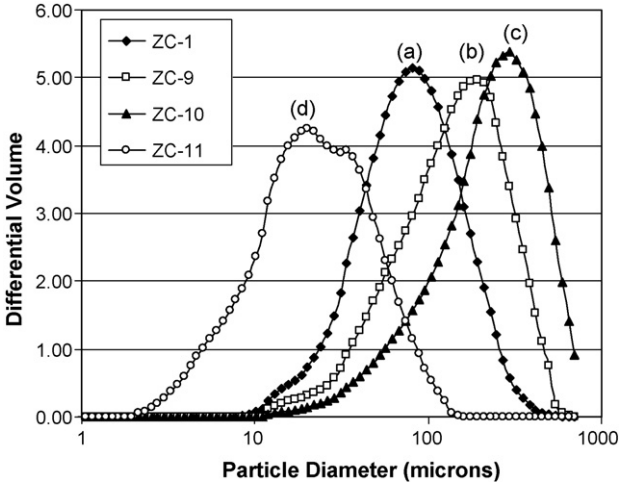

Fig. 10. Particle size distribution of (a) ZC-1, (b) ZC-9, (c) ZC-10, and (d) ZC-11 after 100 hydride/dehydride cycles.

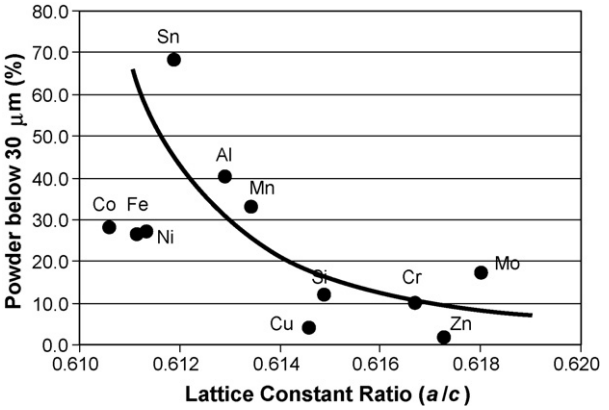

Fig. 12. Percentage of material that passed through a 30-μm sieve after 100 hydride/dehydride cycles vs. lattice constant ratio a/c. A trendline indicates a higher a/c ratio corresponding to a smaller amount of fine particles.

Lattice expansions from the hydride formation of $ZrCr_2$ having a predominantly C14 structure with partial substitution of Cr with Mn, Fe, Co, Ni, and Cu have been reported before [40]. Both the volume expansion ($\Delta V/V$) and volume expansion per stored hydrogen ($\Delta V/VN_H$) were compared to the pulverization data obtained from this study, but no obvious correlation can be established. Both $\Delta V/V$ and $\Delta V/VN_H$ values increase as part of chromium was replaced by one of the transition elements. The increases are related to the degree of structural disorder of the hydride and do not participate in the pulverization process, as is the case with the $LaNi_5$ alloy family, where a larger lattice expansion correlated to a higher PCT hysteresis, and then to a higher pulverization rate [65].

4. Conclusions

The same correlation between PCT hysteresis and particle pulverization can be established for both AB2 alloys having a predominantly C14 crystal structure and AB5 hydrogen storage alloys. A higher PCT hysteresis, implying higher energy barrier between metal and hydride phases, will increase the tension in the alloy during the hydriding process and cause the metal alloy to break more easily. This conclusion may be generalized to other alloy structures without measurable a/c ratios, such as alloys with a predominantly C15 structure. The C14 structure differs from the AB5 alloy in its preference of a flatter unit cell for a lower pulverization rate. Also, no correlation between the extent of lattice expansion and pulverization rate can be established.

References

[1] A.R. Ubbelohde, Proc. Roy. Soc. Lond. A159 (1937) 295.
[2] N.A. Scholtus, W.K. Hall, J. Chem. Phys. 39 (1963) 868.
[3] B.J. Makenas, H.K. Birnbaum, Acta Metall. Mater. 28 (1980) 979.
[4] R. Balasubramaniam, Acta Metall. Mater. 41 (1993) 3341.
[5] R.B. Schwarz, A.G. Khachaturyan, Phys. Rev. Lett. 74 (1995) 2523.
[6] R.B. Schwarz, A.G. Khachaturyan, Acta Mater. 54 (2006) 313.
[7] E. Rabkin, V.M. Skripnyuk, Scripta Mater. 49 (2003) 477.
[8] C. Lexcellent, G. Gondor, Intermetallics 15 (2007) 934.
[9] T.B. Flanagan, J.D. Clewley, J. Less-Common Met. 83 (1982) 127.
[10] T.B. Flanagan, B.S. Bowerman, G.E. Biehl, Scripta Metal. 14 (1980) 443.
[11] J.R. Lacher, Proc. Roy. Soc. Lond. A161 (1937) 525.
[12] C. Wagner, Z. Physik. Chem. 193 (1944) 386.
[13] S. Fang, Z. Zhou, J. Zhang, M. Yao, F. Feng, D.O. Northwood, Int. J. Hydrogen Energy 25 (2000) 143.
[14] S. Fang, Z. Zhou, J. Zhang, M. Yao, F. Feng, D.O. Northwood, J. Alloys Compd. 293–295 (1999) 10.
[15] F. Feng, M. Gang, D.O. Northwood, Comput. Mater. Sci. 23 (2003) 291.
[16] S. Qian, D.O. Northwood, Int. J. Hydrogen Energy 13 (1988) 25.
[17] T.B. Flanagan, C.-N. Park, W.A. Oates, Prog. Solid State Chem. 23 (1995) 291.
[18] Y. Osumi, Suiso-kyuzo-goukin no Syurui to Sono, new ed., Agune Technology Center, Tokyo, Japan, 1999, p. 218.
[19] Y. Osumi, H. Suzuki, A. Kato, K. Oguro, S. Kawai, M. Kaneko, J. Less-Common Met. 89 (1983) 287.
[20] S.R. Ovshinsky, M.A. Fetcenko, J. Ross, Science 260 (1993) 176.
[21] B.S. Chao, R.C. Young, S.R. Ovshinsky, D.A. Pawlik, B. Huang, J.S. Im, B.C. Chakoumakos, Mater. Res. Soc. Symp. Proc. 575 (2000) 193.
[22] Z. Shi, S. Chumbley, F.C. Laabs, J. Alloys Compd. 312 (2000) 41.
[23] M. Yoshida, E. Akiba, J. Alloys Compd. 224 (1995) 121.
[24] O.L. Makarova, I.N. Goncharenko, F. Bourée, Phys. Rev. B67 (2003) 134418.
[25] P. Fisher, W. Hälg, L. Schlapbach, Th. von Wadkirch, Helv. Phys. Acta 51 (1978) 4.
[26] D. Shaltiel, I. Jacob, D. Davidov, J. Less-Common Met. 53 (1977) 117.
[27] D.G. Ivey, D.O. Northwood, J. Mater. Sci. 18 (1983) 321.
[28] D. Fruchart, A. Rouault, C.B. Shoemaker, D.P. Shoemaker, J. Less-Common. Met. 73 (1980) 363.
[29] S. Kanazawa, Y. Kaneno, H. Inoue, W.-Y. Kim, T. Takasugi, Intermetallics 10 (2002) 783.
[30] J. Sun, B. Jiang, Philos. Mag. 84 (2004) 3133.
[31] X.-Q. Chen, W. Wolf, R. Podloucky, P. Rogl, Phys. Rev. B 71 (2005) 174101.
[32] I. Jacob, A. Stern, A. Moran, D. Shaltiel, D. Davidov, J. Less-Common Met. 73 (1980) 369.
[33] J. Park, J. Lee, J. Less-Common Met. 160 (1990) 259.
[34] M.H. Mendelsohn, D.M. Gruen, J. Less-Common Met. 78 (1981) 275.
[35] T. Riesterer, P. Kofel, J. Osterwalder, L. Schlapbach, J. Less-Common Met. 101 (1984) 221.
[36] A. Perevesenzew, E. Lanzel, O.J. Eder, E. Tuscher, P. Weinzierl, J. Less-Common Met. 143 (1988) 39.
[37] M. Bououdina, J.L. Soubeyroux, D. Fruchart, Int. J. Hydrogen Energy 22 (1997) 329.
[38] O. Zhou, Q. Yao, X. Sun, Q. Gu, J. Sun, Chin. J. Nonferr. Met. 16 (2006) 1603.
[39] O. Zhou, Q. Yao, J. Sun, Acta Metall. Sin. 42 (2006) 979.
[40] J.L. Soubeyroux, M. Bououdina, D. Fruchart, L. Pontonnier, J. Alloys Compd. 219 (1995) 48.
[41] I. Jacob, D. Davidov, D. Shaltiel, J. Magn. Magn. Mater. 20 (1980) 226.
[42] V.K. Sinha, G.Y. Yu, W.E. Wallace, J. Less-Common. Met. 106 (1985) 67.
[43] D.G. Ivey, D.O. Northwood, J. Less-Common. Met. 115 (1986) 295.
[44] D.G. Ivey, D.O. Northwood, Int. J. Hydrogen Energy 11 (1986) 583.
[45] S. Qian, D.O. Northwood, J. Less-Common Met 147 (1989) 149.
[46] X.M. Burany, D.O. Northwood, J. Less-Common Met. 170 (1991) 27.
[47] A. Drašner, Ž. Blažina, J. Less-Common Met. 168 (1991) 289.
[48] A. Jain, R.K. Jain, S. Agarwal, I.P. Jain, J. Int. Hydrogen Energy 32 (2007) 2445.
[49] S. Hirosawa, F. Pourarian, V.K. Sinha, W.E. Wallace, J. Magn. Magn. Mater. 38 (1983) 159.
[50] A. Drašner, Ž. Blažina, J. Less-Common Met. 163 (1990) 151.
[51] Ž. Blažina, A. Drašner, J. Magn. Mag. Mater. 119 (1993) L15.
[52] C.B. Jung, J.H. Kim, K.S. Lee, Nanostruct. Mater. 8 (1997) 1093.
[53] M. Bououdina, J.L. Soubeyroux, D. Fruchart, P. de Rango, J. Alloys Compd. 257 (1997) 82.
[54] A.Y. Esayed, D.O. Northwood, Int. J. Hydrogen Energy 22 (1997) 77.
[55] A. Drašner, Ž. Blažina, J. Less-Common Met. 175 (1991) 103.
[56] M. Bououdina, J.L. Soubeyroux, P. de Rango, D. Fruchart, Int. J. Hydrogen Energy 25 (2000) 1059.
[57] I. Jacob, D. Shaltiel, in: T.N. Verizoglu, W. Seifritz (Eds.), Hydrogen Energy Systems, Pergamon, Oxford, 1979, p.1689.
[58] A. Drašner, Ž. Blažina, J. Alloys Compd. 199 (1993) 101.
[59] Nihon Kinzoku Gakkai, Hi Kagaku Ryouronteki Kinzoku Kagobutu, Maruzen, Tokyo, 1975, p. 296.
[60] R.L. Johnson, R. Hoffmann, Z. Anorg. Allg. Chem. 616 (1992) 105.
[61] J.H. Zhu, P.K. Liaw, C.T. Liu, Mater. Sci. Eng. A239–240 (1997) 260.
[62] H. Nakano, I. Wada, S. Wakao, J. Adv. Sci. 4 (1992) 239.
[63] D.G. Ivey, R.I. Chittim, K.J. Chittim, D.O. Northwood, J. Mater. Energy Syst. 3 (1981) 3.
[64] K.J. Gross, A. Züttel, L. Schlapbach, J. Alloys Compd. 274 (1998) 239.
[65] Y. Osumi, H. Suzuki, A. Kato, K. Oguro, J. Less-Common Met. 89 (1983) 287.